Chapter 12

Nuclear Models

Note to students and other readers: This Chapter is intended to supplement Chapter 5 of Krane's excellent book, "Introductory Nuclear Physics". Kindly read the relevant sections in Krane's book first. This reading is supplementary to that, and the subsection ordering will mirror that of Krane's, at least until further notice.

Many of the ideas and methods we learned in studying atoms and their quantum behaviour, carry over to nuclear physics. However, in some important ways, they are quite different:

1. We don't really know what the nucleon-nucleon potential is, but we do know that it has a central, $V(r)$, and non-central part, $V(\vec{x})$. That is the first complication.

2. The force on one nucleon not only depends on the position of the other nucleons, but also on the distances between the other nucleons! These are called *many-body* forces. That is the second complication.

Let us illustrate this in Figure 12.1, where we show the internal forces governing a ^{3}He nucleus.

Figure 12.1: Theoretical sketch of a ^{3}He nucleus. *This sketch has not been created yet, so feel free to draw it in!*

The potential on the proton at $\vec{x}_1$ is given by:

$$V_{nn}(\vec{x}_2 - \vec{x}_1) + V_{nn}(\vec{x}_3 - \vec{x}_1) + V_{\rm C}(|\vec{x}_2 - \vec{x}_1|) + V_3(\vec{x}_1 - \vec{x}_2, \vec{x}_1 - \vec{x}_3, \vec{x}_2 - \vec{x}_3) \ , \qquad (12.1)$$

where:

Potential term	Explanation
$V_{nn}(\vec{x}_2 - \vec{x}_1)$	2-body strong nuclear force between p at $\vec{x}_1$ and p at $\vec{x}_2$
$V_{nn}(\vec{x}_3 - \vec{x}_1)$	2-body strong nuclear force between p at $\vec{x}_1$ and n at $\vec{x}_3$
$V_{\rm C}(\|\vec{x}_2 - \vec{x}_1\|)$	2-body Coulomb force between p at $\vec{x}_1$ and p at $\vec{x}_2$
$V_3(\cdots)$	3-body force strong nuclear force (more explanation below)

The 2-body forces above follow from our discussion of the strong and Coulomb 2-body forces. However, the 3-body term is a fundamentally different thing. You can think of V_3 as a "polarization" term—the presence of several influences, how 2 acts on 1 in the presence of 3, how 3 acts on 1 in the presence of 2, and how this is also affected by the distance between 2 and 3. It may seem complicated, but it is familiar. People act this way! Person 1 may interact with person 2 in a different way if person 3 is present! These many-body forces are hard to get a grip on, in nuclear physics and in human social interaction. Nuclear theory is basically a phenomenological one based on measurement, and 3-body forces or higher order forces are hard to measure.

Polarization effects are common in atomic physics as well.

Figure 12.2, shows how an electron passing by, in the vicinity of two neutral atoms, polarizes the proximal atom, as well as more distance atoms.

returning to nuclear physics, despite the complication of many-body forces, we shall persist with the development of simple models for nuclei. These models organize the way we think about nuclei, based upon some intuitive guesses. Should one of these guesses have predictive power, that is, it predicts some behaviour we can measure, we have learned something—not the entire picture, but at least some aspect of it. With no fundamental theory, this form of guesswork, phenomenology, is the best we can do.

Figure 12.2: A depiction of polarization for an electron in condensed matter. *This sketch has not been created yet, so feel free to draw it in!*

12.1 The Shell Model

Atomic systems show a very pronounced shell structure. See Figures 12.3 and 12.4.

Figure 12.3: For now, substitute the top figure from Figure 5.1 in Krane's book, p. 118. This figure shows shell-induced regularities of the atomic radii of the elements.

Figure 12.4: For now, substitute the bottom figure from Figure 5.1 in Krane's book, p. 118. This figure shows shell-induced regularities of the ionization energies of the elements.

Nuclei, as well, show a "shell-like" structure, as seen in Figure 12.5.

Figure 12.5: For now, substitute Figure 5.2 in Krane's book, p. 119. This figure shows shell-induced regularities of the $2p$ separation energies for sequences of isotones same N, and $2n$ separation energies for sequences of isotopes.

The peak of the separation energies (hardest to separate) occur when the Z or N correspond to major closed shells. The "magic" numbers, the closed major shells, occur at Z or N: 2, 8, 20, 28, 50, 82, & 126.

The stable magic nuclei

Isotopes	Explanation	Natural abundance (%)
$^{3}_{2}\mathrm{He}_{1}$	magic Z	1.38×10^{-4}
$^{4}_{2}\mathrm{He}_{2}$	doubly magic	99.99986
$^{15}_{7}\mathrm{N}_{8}$	magic N	0.366
$^{16}_{8}\mathrm{O}_{8}$	doubly magic	99.76
$^{40}_{20}\mathrm{Ca}_{20}$	doubly magic	96.94
$^{42-48}_{20}\mathrm{Ca}_{20}$	magic Z	
$^{50}_{22}\mathrm{Ti}_{28}$	magic N	5.2
$^{52}_{24}\mathrm{Cr}_{28}$	magic N	83.79
$^{54}_{26}\mathrm{Fe}_{28}$	magic N	5.8
^{86}Kr, ^{87}Rb, ^{88}Sr, ^{89}Y, ^{90}Zr, ^{92}Mo	magic $N = 50$	
⋮	⋮	⋮
$^{208}_{82}\mathrm{Pb}_{126}$	doubly magic	52.3
$^{209}_{83}\mathrm{Bi}_{126}$	magic N	100, $t_{1/2} = 19 \pm 2 \times 10^{18}$ y

The Shell-Model idea

A nucleus is composed of a "core" that produces a potential that determines the properties of the "valence" nucleons. These properties determine the behaviour of the nucleus much in the same way that the valance electrons in an atom determine its chemical properties.

The excitation levels of nuclei appears to be chaotic and inscrutable. However, there is order to the mess! Figure 12.6 shows the energy levels predicted by the shell model using ever-increasing sophistication in the model of the "core" potential. The harmonic oscillator potential as well as the infinite well potential predict the first few magin numbers. However, one must also include details of the profile of the nuclear skin, as well as introduce a spin-orbit coupling term, before the shells fall into place. In the next section we discuss the various components of the modern nuclear potential.

Details of the modern nuclear potential

A valence nucleon (p or n) feels the following central strong force from the core:

$$V_n(r) = \frac{-V_0}{1 + \exp\left(\frac{r - R_N}{t}\right)} \tag{12.2}$$

It is no coincidence that the form of this potential closely resembles the shape of the nucleus as determined by electron scattering experiments. The presence of the nucleons in the core, provides the force, and thus, the force is derived directly from the shape of the core.

Figure 12.6: The shell model energy levels. See Figures 5.4 (p. 121) and 5.5 p. 123 in Krane.

In addition to the "bulk" attraction in (12.2), there is a symmetry term when there is an imbalance of neutrons and protons. This symmetry term is given by:

$$V_{\rm S} = \frac{a_{\rm sym}}{A(A+1)}\left[\pm 2(N-Z)A + A - (N-Z)^2\right] \ , \tag{12.3}$$

with the plus sign is for a valence neutron and the negative sign for a valence proton. The form of this potential can be derived from the parametric fit to the total binding energy of a nucleus given by (**??**).

The paramters of the potential described above, are conventionally given as:

Parameter	Value	Interpretation
V_0	57 MeV	Potential depth of the core
R_N	$1.25A^{1/3}$	Nuclear radius
t	0.65 fm	Nuclear skin depth
$a_{\rm sym}$	16.8 MeV	Symmetry energy
a_{so}	1 fm	Spin-ordit coupling (discussed below)

If the valence nucleon is a proton, an addition central Coulomb repulsion must be applied:

$$V_{\rm C}(r) = \frac{Ze^2}{4\pi\epsilon_0}\int {\rm d}\vec{x}'\rho_p(r')\frac{1}{|\vec{x}-\vec{x}'|} = \frac{Ze^2}{4\pi\epsilon_0}\frac{2\pi}{r}\int {\rm d}r' r'\rho_p(r')\left[(r+r') - |r-r'|\right] \ . \tag{12.4}$$

Recall that the proton density is normalized to unity by

$$1 \equiv \int \mathrm{d}\vec{x}' \rho_p(r') = 4\pi \int \mathrm{d}r' r'^2 \rho_p(r') \ .$$

Simple approximations to (12.4) treat the charge distribution as a uniform sphere with radius R_N. That is:

$$\rho_p(r) \approx \frac{3}{4\pi R_N^3} \Theta(R - r) \ .$$

However, a more sophisticated approach would be to use the nuclear shape suggested by (12.2), that is:

$$\rho_p(r) = \frac{\rho_0}{1 + \exp\left(\frac{r - R_N}{t}\right)} \ ,$$

determining ρ_0 from the normalization condition above.

The spin-orbit potential

The spin-orbit potential has the form:

$$V_{so}(\vec{x}) = -\frac{a_{so}^2}{r} \frac{\mathrm{d}V_n(r)}{\mathrm{d}r} \langle \vec{l} \cdot \vec{s} \rangle \ . \tag{12.5}$$

The radial derivative in the above equation is only meant to be applied where the nuclear density is changing rapidly.

Evaluating the spin-orbit term

Recall, $\vec{j} = \vec{l} + \vec{s}$. Hence, $\vec{j}^2 = \vec{l}^2 + 2\vec{l} \cdot \vec{s} + \vec{s}^2$. Thus, $\vec{l} \cdot \vec{s} = (1/2)(\vec{j}^2 - \vec{l}^2 - \vec{s}^2)$, and $\langle \vec{l} \cdot \vec{s} \rangle = (1/2)[j(j+1) - l(l+1) - s(s+1)]$.

The valence nucleon has spin-1/2. To determine the splitting of a given l into $j = l \pm \frac{1}{2}$ levels, we calculate, therefore:

$$\begin{aligned}
\langle \vec{l} \cdot \vec{s} \rangle_{j=l+\frac{1}{2}} &= [(l + 1/2)(l + 3/2) - l(l+1) - 3/4]/2 \\
&= l/2 \\
\langle \vec{l} \cdot \vec{s} \rangle_{j=l-\frac{1}{2}} &= [(l - 1/2)(l + 1/2) - l(l+1) - 3/4]/2 \\
&= -(l+1)/2 \\
\langle \vec{l} \cdot \vec{s} \rangle_{j=l+\frac{1}{2}} - \langle \vec{l} \cdot \vec{s} \rangle_{j=l-\frac{1}{2}} &= (2l+1)/2
\end{aligned} \tag{12.6}$$

$V_{so}(r)$ is negative, and so, the higher $j = l + \frac{1}{2}$ (orbit and spin angular momenta are aligned) is more tightly bound.

The shape of this potential is show, for a valence neutron in Figure 12.7, and for a valence proton in Figure 12.8. For this demonstration, the core nucleus was ^{208}Pb. The l in the figures, to highlight the spin-orbit coupling, was chosen to be $l = 10$.

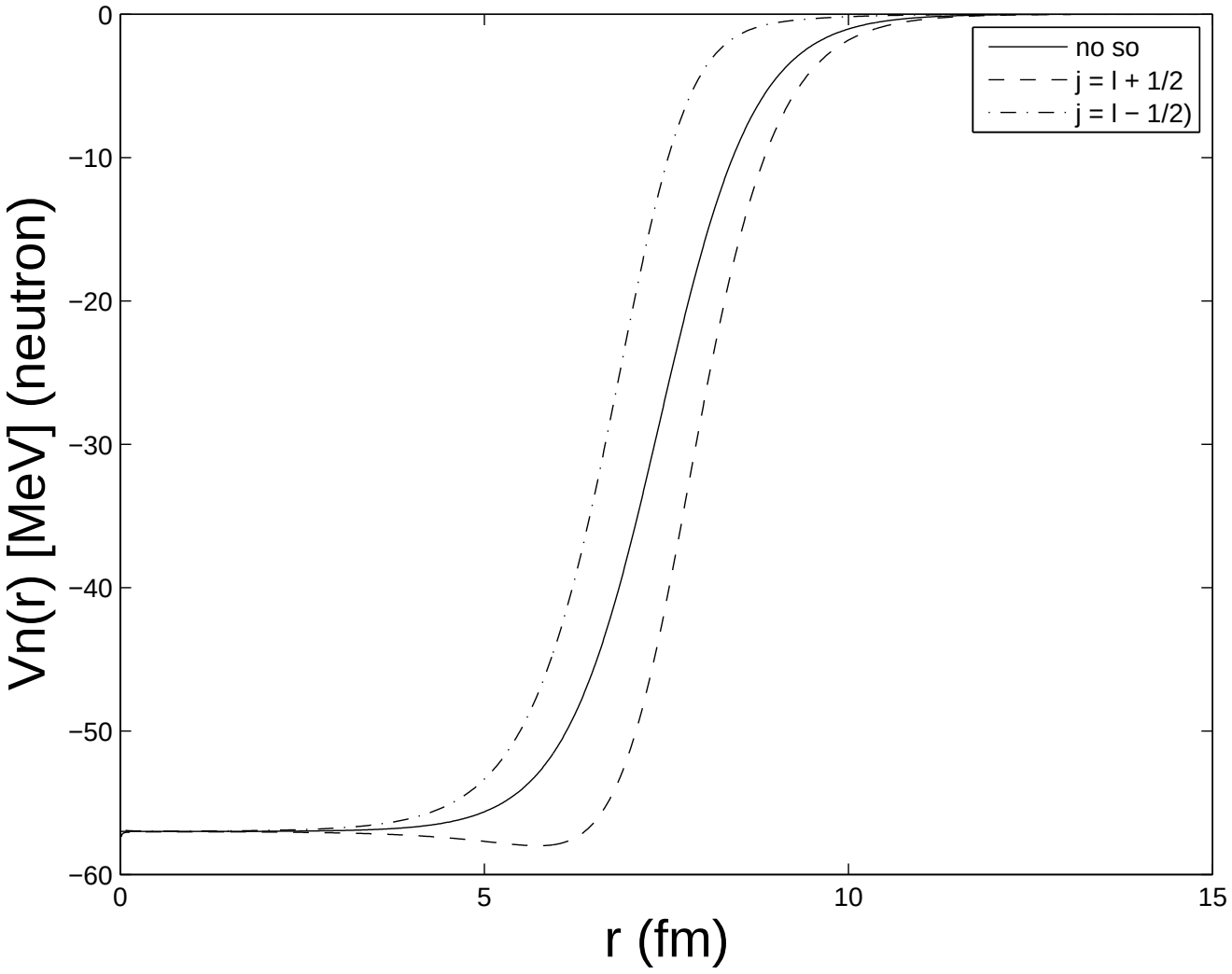

Figure 12.7: The potential of a ^{208}Pb nucleus as seen by a single valence neutron.

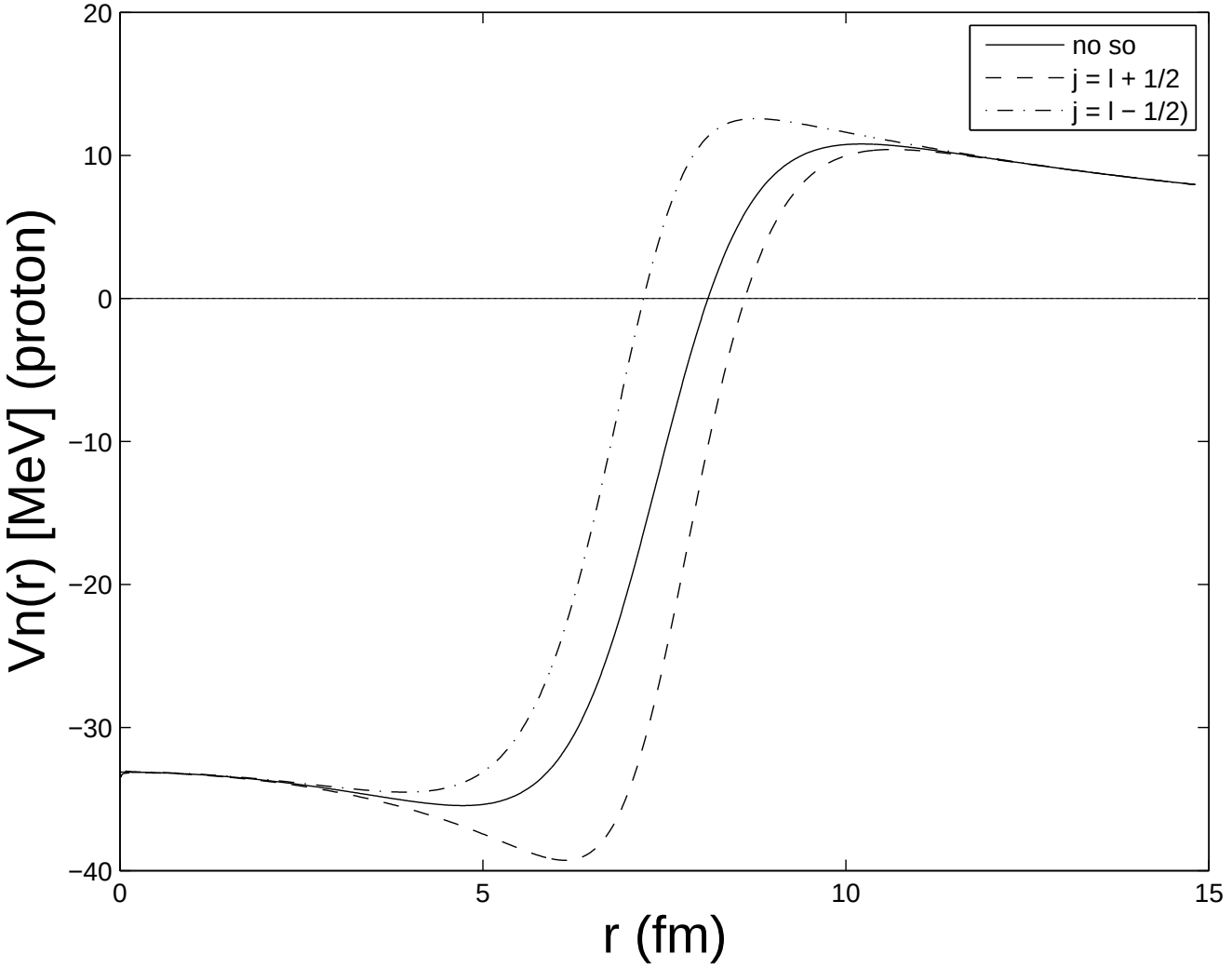

Figure 12.8: The potential of a ^{208}Pb nucleus as seen by a single valence proton. Note the effect of the Coulomb potential on the the potential near the origin (parabolic shape there), as well as the presence of the Coulomb barrier.

Determining the ground state I^π in the shell model

The spin and parity assignment may be determined by considering the nuclear potential described so far, plus one additional idea, the "Extreme Independent Particle Model" (EIPM). The EIPM is an addendum to the shell model idea, and it is expressed as follows. *All the characteristics of a given nucleus are determined by the unpaired valence nucleons. All pairs of like nucleons cancel one another's spins and parities.*

Applying EIPM for the example of two closely related nuclei is demonstrated in Figure 12.9.

Figure 12.9: A demonstration of the spin and parity assignment for ^{15}O and ^{17}O. $I^\pi(^{15}\mathrm{O}) = \frac{1}{2}^-$, while $I^\pi(^{17}\mathrm{O}) = \frac{5}{2}^+$. *This sketch has not been created yet, so feel free to draw it in!*

Another demonstration of the success of the EIPM model is to consider the isotopes of O.

Isotope of O	I^π, measured	I^π, EIPM prediction	decay mode	$t_{1/2}$/abundance
^{12}O	0^+ (est)	0^+	$2p$	$\approx 10^{-21}$ s
^{13}O	$\frac{3}{2}^-$	$\frac{3}{2}^-$	β^+, p	8.6 ms
^{14}O	0^+	0^+	γ, β^+	70.60 s
^{15}O	$\frac{1}{2}^-$	$\frac{1}{2}^-$	ε, β^+	2.037 m
^{16}O	0^+	0^+		99.757%
^{17}O	$\frac{5}{2}^+$	$\frac{5}{2}^+$		0.038%
^{18}O	0^+	0^+		0.205%
^{19}O	$\frac{5}{2}^+$	$\frac{5}{2}^+$	β^-, γ	26.9 s
^{20}O	0^+	0^+	β^-, γ	13.5 s
^{21}O	?	$\frac{5}{2}^+$	β^-, γ	3.4 s
^{22}O	0^+ (est)	0^+	β^-, γ	2.2 s
^{23}O	?	$\frac{1}{2}^+$	β^-, n	0.08 s
^{24}O	0^+ (est)	0^+	β^-, γ, n	65 ms

Other successes ...

Isotope	I^π
$^{13}_{5}\mathrm{Be}_8$	$\frac{3}{2}^-$
$^{14}_{6}\mathrm{C}_8$	0^+
$^{15}_{7}\mathrm{N}_8$	$\frac{1}{2}^-$
$^{16}_{8}\mathrm{O}_8$	0^+
$^{17}_{8}\mathrm{F}_8$	$\frac{5}{2}^+$
$^{18}_{10}\mathrm{Ne}_8$	0^+

EIPM prediction of the magnetic moment of the nucleus

The shell model, and its EIPM interpretation, can be tested by measuring and calculating the magnetic moment of a nucleus. Thus, the last unpaired nucleon determines the magnetic moment of the entire nucleus. Recall from Chapter 10, the definition of magnetic moment, μ, of a nucleus:

$$\mu = \mu_{\mathrm{N}}(g_l l_z + g_s s_z) \ , \tag{12.7}$$

where

Symbol	Meaning	Value
$\mu_{\rm N}$	Nuclear magnetron	$5.05078324(13) \times 10^{-27}$ J/T
g_l	Orbital gyromagnetic ratio	0 (neutron), 1 (proton)
g_s	Spin gyromagnetic ratio	$-3.82608545(46)$ (neutron) 5.585694713(90) (proton)
l_z	Maximum value of m_l	$j_z = \max(m_l)$
s_z	Maximum value of m_s	$s_z = \max(m_s) = 1/2$

However, neither $\vec{l}$ nor $\vec{s}$ is precisely defined for nuclei (recall the Deuteron) due to the strong spin-orbit coupling. Consequently, l_z and s_z can not be known precisely. However, total angular momentum, $\vec{j}$ and its maximum z-projection, j_z are precisely defined, and thus measurable.

Since $j_z = l_z + s_z$, we may rewrite (12.7) as:

$$\mu = \mu_{\rm N}(g_l j_z + (g_s - g_l)s_z) \ . \tag{12.8}$$

Computing the expectation value (*i.e.* the measured value) of μ gives:

$$\langle\mu\rangle = \mu_{\rm N}(g_l j + (g_s - g_l)\langle s_z\rangle) \ . \tag{12.9}$$

Since $\vec{j}$ is the only measurable vector in the nucleus, we can determine $\langle s_z\rangle$ from its projection along $\vec{j}$.

Thus, using projection vector language:

$$\begin{aligned}
\vec{s}_j &= \vec{j}\frac{(\vec{s}\cdot\vec{j})}{\vec{j}\cdot\vec{j}} \ , \\
s_z = \hat{z}\cdot\vec{s}_j &= j_z\frac{\vec{s}\cdot\vec{j}}{\vec{j}\cdot\vec{j}} \ , \\
\langle s_z\rangle &= j\frac{\langle\vec{s}\cdot\vec{j}\rangle}{j(j+1)} \ , \\
\langle s_z\rangle &= \frac{\langle\vec{s}\cdot\vec{j}\rangle}{(j+1)} \ , \\
\langle s_z\rangle &= \frac{\langle\vec{j}\cdot\vec{j}\rangle - \langle\vec{l}\cdot\vec{l}\rangle + \langle\vec{s}\cdot\vec{s}\rangle}{2(j+1)} \ , \\
\langle s_z\rangle &= \frac{j(j+1) - l(l+1) + s(s+1)}{2(j+1)} \ , \\
\langle s_z\rangle_{j=l+1/2} &= 1/2 \ , \\
\langle s_z\rangle_{j=l-1/2} &= -\frac{j}{2(j+1)} \ .
\end{aligned} \tag{12.10}$$

Substituting the results of (12.10) into (12.9) gives:

$$\begin{aligned} \langle\mu\rangle_{j=l+1/2} &= \mu_{\rm N}\left[g_l(j-\tfrac{1}{2})+\tfrac{1}{2}g_s\right] \\ \langle\mu\rangle_{j=l-1/2} &= \mu_{\rm N}\left[g_l\frac{j(j+\frac{3}{2})}{(j+1)}-\frac{g_s}{2}\frac{j}{(j+1)}\right] \end{aligned} \tag{12.11}$$

Comparisons of measurements with theory are given in Figure 12.10, for odd-neutron and odd-proton nuclei. These nuclei are expected to give the best agreement with the EIPM. The theoretical lines are know as Schmidt lines, honoring the first person who developed the theory. Generally, the trends in the data are followed by the Schmidt lines, though the measured data is significantly lower. The reason for this is probably a "polarization effect", where the intrinsic spin of the odd nucleon is shielded by the other nucleons in the nucleus as well as the virtual exchange mesons. This is very similar to a charged particle entering a condensed medium and polarizing the surrounding atoms, thereby reducing the effect of its charge. This can be interpreted as a reduction in charge by the surrounding medium. (The typical size of this reduction is only about 1–2%. However, in a nucleus, the forces are much stronger, and hence, so is the polarization. The typical reduction factor applied to the nucleons are g_s (in nucleus) $\approx 0.6 g_s$ (free).

Figure 12.10: *See Krane's Figure 5.9, p. 127*

Shell model and EIPM prediction of the quadrupole moment of the nucleus

Recall the definition of the quadrupole moment of a nucleus, given in (**??**) namely:

$$Q = \int {\rm d}\vec{x}\ \psi_N^*(\vec{x})(3z^2-r^2)\psi_N(\vec{x})\ .$$

A quantum-mechanical calculation of the quadrupole moment for a single odd proton, by itself in a subshell, is given by:

$$\langle Q_{\rm sp}\rangle = -\frac{2j-1}{2(j+1)}\langle r^2\rangle \ . \tag{12.12}$$

When a subshell contains more than one particle, all the particles in that subshell can, in principle, contribute to the quadrupole moment. The consequence of this is that the quadrupole moment is given by:

$$\langle Q\rangle = \langle Q_{\rm sp}\rangle \left[1 - 2\frac{n-1}{2j-1}\right] \ , \tag{12.13}$$

where n is the occupancy of that level. We can rewrite (12.13) in to related ways:

$$\begin{aligned} \langle Q\rangle(n) &= \langle Q_{\rm sp}\rangle \left[\frac{2(j-n)+1}{2j-1}\right] \ , \\ \langle Q\rangle(n_0) &= \langle Q_{\rm sp}\rangle \left[\frac{-2(j-n_0)-1}{2j-1}\right] \ , \end{aligned} \tag{12.14}$$

where $n_0 = 2j+1-n$ is the number of "holes" in the subshell. Thus we see that (12.14) predicts $\langle Q\rangle(n_0 = n) = -\langle Q\rangle(n)$. The interpretation is that "holes" have the same magnitude quadrupole moment as if there were the equivalent number of particles in the shell, but with a difference in sign. Krane's Table 5.1 (p. 129) bears this out, despite the generally poor agreement in the absolute value of the quadrupole moment as predicted by theory.

Even more astonishing is the measured quadrupole moment for single neutron, single-neutron hole data. There is no theory for this! Neutrons are not charged, and therefore, if Q were determined by the "last unpaired nucleon in" idea, Q would be zero for these states. It might be lesser in magnitude, but it is definitely not zero!

There is much more going on than the EIPM or shell models can predict. These are collective effects, whereby the odd neutron perturb the shape of the nuclear core, resulting in a measurable quadrupole moment. EIPM and the shell model can not address this physics. It is also known that the shell model prediction of quadrupole moments fails catastrophically for $60 < Z < 80$, $Z > 90$ $90 < N < 120$ and $N > 140$, where the measured moments are an order of magnitude greater. This is due to collective effects, either multiple particle behavior or a collective effect involving the entire core. We shall investigate these in due course.

Shell model predictions of excited states

If the EIPM were true, we could measure the shell model energy levels by observing the decays of excited states. Recall the shell model energy diagram, and let us focus on the lighter nuclei.

Figure 12.11: The low-lying states in the shell model

Let us see if we can predict and compare the excited states of two related light nuclei: ${}^{17}_{8}\mathrm{O}_9 = [{}^{16}_{8}\mathrm{O}_8] + 1n$, and ${}^{19}_{9}\mathrm{F}_8 = [{}^{16}_{8}\mathrm{O}_8] + 1p$.

Figure 12.12: The low-lying excited states of ${}^{17}_{8}\mathrm{O}_9$ and ${}^{19}_{9}\mathrm{F}_8$. Krane's Figure 5.11, p. 131

The first excited state of ${}^{17}_{8}\mathrm{O}_9$ and ${}^{19}_{9}\mathrm{F}_8$ has $I^\pi = 1/2^+$. This is explained by the EIPM interpretation. The "last in" unpaired nucleon at the $1d_{5/2}$ level is promoted to the $2s_{1/2}$ level, vacating the $1d$ shell. The second excited state with $I^\pi = 1/2^-$ does not follow the EIPM model. Instead, it appears that a core nucleon is raised from the $1p_{1/2}$ level to the $1d_{5/2}$ level, joining another nucleon there and cancelling spins. The $I^\pi = 1/2^-$ is determined by the unpaired nucleon left behind. Nor do the third and fourth excited states follow the EIPM prescription. The third and fourth excited states seem to be formed by a core nucleon raised from the $1p_{1/2}$ level to the $2s_{1/2}$ level, leaving three unpaired nucleons. Since I is formed from the coupling of j's of $1/2$, $1/2$ and $5/2$, we expect $3/2 \leq I \leq 7/2$. $3/2$ is the lowest followed by $5/2$. Not shown, but expected to appear higher up would be the $7/2$. The parity is negative, because parity is multiplicative. Symbolically, $(-1)^p \times (-1)^d \times (-1)^s = -1$. Finally, the fifth excited state does follow the EIPM prescription, raising the "last in" unbound nucleon to $d_{3/2}$ resulting in an $I^\pi = 3/2^+$.

Hints of collective structure

Krane's discussion on this topic is quite good.

Figure 12.13: The low-lying excited states of ${}^{41}_{20}\mathrm{Ca}_{21}$, ${}^{41}_{21}\mathrm{Sc}_{20}$, ${}^{43}_{20}\mathrm{Ca}_{23}$, ${}^{43}_{21}\mathrm{Sc}_{22}$, ${}^{43}_{22}\mathrm{Ti}_{21}$. Krane's figure 5.12, p. 132

Verification of the shell model

Krane has a very interesting discussion on a demonstration of the validity of the shell model by investigating the behavior of s states in heavy nuclei. In this demonstration, the difference in the proton charge distribution (measured by electrons), is compared for ${}^{205}_{81}\mathrm{Tl}_{124}$ and ${}^{206}_{82}\mathrm{Pb}_{124}$.

$$\rho_{\mathrm{p}}^{{}^{205}_{81}\mathrm{Tl}_{124}}(r) - \rho_{\mathrm{p}}^{{}^{206}_{82}\mathrm{Pb}_{124}}(r)$$

^{206}Pb has a magic number of protons and 124 neutrons while ^{205}Tl has the same number of neutrons and 1 less proton. That proton is in an $s_{1/2}$ orbital. So, the measurement of the charge density is a direct investigation of the effect of an unpaired proton coursing though the tight nuclear core, whilst on its s-state meanderings.

12.2 Even-Z, even-N Nuclei and Collective Structure

All even/even nuclei are $I^\pi = 0^+$, a clear demonstration of the effect of the pairing force.

All even/even nuclei have an anomalously small 1st excited state at 2^+ that can not be explained by the shell model (EIPM or not). Read Krane pp. 134–138.

Consult Krane's Figure 5.15a, and observe that, except near closed shells, there is a smooth downward trend in $E(2^+)$, the binding energy of the lowest 2^+ states. Regions $150 < A < 190$ and $A > 220$ seem very small and consistent.

Quadrupole moment systematics

Q_2 is small for $A < 150$. Q_2 is large and negative for $150 < A < 190$ suggesting an *oblate* deformation

Consult Krane's Figure 5.16b: The regions between $150 < A < 190$ and $A > 220$ are markedly different. Now, consult Krane's Figure 5.15b that shows the ratio of $E(4^+)/E(2^+)$. One also notes something "special about the regions:$150 < A < 190$ and $A > 220$.

All this evidence suggests a form of "collective behavior" that is described by the *Liquid Drop Model* (LDM) of the nucleus.

12.2.1 The Liquid Drop Model of the Nucleus

In the the Liquid Drop Model is familiar to us from the semi-empirical mass formula (SEMF). When we justified the first few terms in the SEMF, we argued that the bulk term and the surface term were characteristics of a cohesive, attractive mass of nucleons, all in contact with each other, all in motion, much like that of a fluid, like water. Adding a nucleon liberates a certain amount of energy, identical for each added nucleon. The gives rise to the bulk term. The bulk binding is offset somewhat by the deficit of attraction of a nucleon at or near the surface. That nucleon has fewer neighbors to provide full attraction. Even the Coulomb repulsion term can be considered to be a consequence of this model, adding in the extra physics of electrostatic repulsion. Now we consider that this "liquid drop" may have collective (many or all nucleons participating) excited states, in the quantum mechanical sense[1].

These excitations are known to have two distinct forms:

- Vibrational excitations, about a spherical or ellipsoidal shape. All nucleons participate in this behavior. (This is also known as photon excitation.)
- Rotational excitation, associated with rotations of the entire nucleus, or possibly only the valence nucleons participating, with perhaps some "drag" on a non-rotating spherical core. (This is also known as roton excitation.)

Nuclear Vibrations (Phonons)

Here we characterize the nuclear radius as have a temporal variation in polar angles in the form:

$$R(\theta, \phi, t) = R_{\text{avg}} + \sum_{\lambda=1}^{\Lambda} \sum_{\mu=-\lambda}^{\lambda} \alpha_{\lambda\mu}(t) Y_{\lambda\mu}(\theta, \phi) \ , \tag{12.15}$$

[1]A classical liquid drop could be excited as well, but those energies would appears not to be quantized. (Actually, they are, but the quantum numbers are so large that the excitations appear to fall on a continuum.

Here, $R_{\rm avg}$ is the "average" radius of the nucleus, and $\alpha_{\lambda\mu}(t)$ are temporal deformation parameters. Reflection symmetry requires that $\alpha_{\lambda,-\mu}(t) = \alpha_{\lambda\mu}(t)$. Equation (12.15) describes the surface in terms of sums total angular momentum components $\vec{\lambda}\hbar$ and their z-components, $\mu\hbar$. The upper bound on λ is some upper bound Λ. Beyond that, presumably, the nucleus can not longer be bound, and flies apart. If we insist that the nucleus is an incompressible fluid, we have the further constraints:

$$\begin{aligned} V_N &= \frac{4\pi}{3} R_{\rm avg}^3 \\ 0 &= \sum_{\lambda=1}^{\Lambda} |\alpha_{\lambda,0}(t)|^2 + 2\sum_{\lambda=1}^{\Lambda}\sum_{\mu=1}^{\lambda} |\alpha_{\lambda\mu}(t)|^2 \end{aligned} \tag{12.16}$$

The λ deformations are shown in Figure 12.14 for $\lambda = 1, 2, 3$.

Figure 12.14: In this figure, nuclear surface deformations are shown for $\lambda = 1, 2, 3$

Dipole phonon excitation

The $\lambda = 1$ formation is a *dipole* excitation. Nuclear deformation dipole states are not observed in nature, because a dipole excitation is tantamount to a oscillation of the center of mass.

Quadrupole phonon excitation

The $\lambda = 2$ excitation is called a *quadrupole excitation* or a *quadrupole phonon excitation*, the latter being more common. Since $\pi = (-1)^\lambda$, the parity of the quadrupole phonon excitation is always positive, and it's $I^\pi = 2^+$.

Octopole phonon excitation

The $\lambda = 3$ excitation is called an *octopole excitation* or a *octopole phonon excitation*, the latter being more common. Since $\pi = (-1)^\lambda$, the parity of the octopole phonon excitation is always negative, and it's $I^\pi = 3^-$.

Two-quadrupole phonon excitation

Now is gets interesting! These quadrupole spins add in the quantum mechanical way. Let us enumerate all the apparently possible combinations of $|\mu_1\rangle$ and $|\mu_2\rangle$ for a two photon excitation:

$\mu = \mu_1 + \mu_2$	Combinations	d	$\mu_{\lambda=4}$	$\mu_{\lambda=3}$	$\mu_{\lambda=2}$	$\mu_{\lambda=1}$	$\mu_{\lambda=0}$
4	$\|2\rangle\|2\rangle$	1	y				
3	$\|2\rangle\|1\rangle, \|1\rangle\|2\rangle$	2	y	y			
2	$\|2\rangle\|0\rangle, \|1\rangle\|1\rangle, \|0\rangle\|2\rangle$	3	y	y	y		
1	$\|2\rangle\|\text{-}1\rangle, \|1\rangle\|0\rangle, \|0\rangle\|1\rangle, \|\text{-}1\rangle\|2\rangle$	4	y	y	y	y	
0	$\|2\rangle\|\text{-}2\rangle, \|1\rangle\|\text{-}1\rangle, \|0\rangle\|0\rangle, \|\text{-}1\rangle\|1\rangle, \|\text{-}2\rangle\|2\rangle$	5	y	y	y	y	y
-1	$\|1\rangle\|\text{-}2\rangle, \|0\rangle\|\text{-}1\rangle, \|\text{-}1\rangle\|0\rangle, \|\text{-}2\rangle\|1\rangle$	4	y	y	y	y	
-2	$\|0\rangle\|\text{-}2\rangle, \|\text{-}1\rangle\|\text{-}1\rangle, \|\text{-}2\rangle\|0\rangle$	3	y	y	y		
-3	$\|\text{-}1\rangle\|\text{-}2\rangle, \|\text{-}2\rangle\|\text{-}1\rangle$	2	y	y			
-4	$\|\text{-}2\rangle\|\text{-}2\rangle$	1	y				
		$\sum d = 25$	9	7	5	3	1

It would appear that we could make two-quadrupole phonon states with $I^\pi = 4^+, 3^-, 2^+, 1^-, 0^+$. However, phonons are unit spin excitations, and follow Bose-Einstein statistics, Therefore, only symmetric combinations can occur. Accounting for this, as we have done following, leads us to conclude that the only possibilities are: $I^\pi = 4^+, 2^+, 0^+$.

$\mu = \mu_1 + \mu_2$	Symmetric combinations	d	$\mu_{\lambda=4}$	$\mu_{\lambda=2}$	$\mu_{\lambda=0}$
4	$\|2\rangle\|2\rangle$	1	y		
3	$(\|2\rangle\|1\rangle+\|1\rangle\|2\rangle)$	1	y		
2	$(\|2\rangle\|0\rangle+\|0\rangle\|2\rangle)$, $\|1\rangle\|1\rangle$	2	y	y	
1	$(\|2\rangle\|\text{-}1\rangle+\|\text{-}1\rangle\|2\rangle)$, $(\|1\rangle\|0\rangle+\|0\rangle\|1\rangle)$	2	y	y	
0	$(\|2\rangle\|\text{-}2\rangle+\|\text{-}2\rangle\|2\rangle)$, $(\|1\rangle\|\text{-}1\rangle+\|\text{-}1\rangle\|1\rangle)$, $\|0\rangle\|0\rangle$	3	y	y	y
-1	$(\|1\rangle\|\text{-}2\rangle+\|\text{-}2\rangle\|1\rangle)$, $(\|0\rangle\|\ 1\rangle+\|\text{-}1\rangle\|0\rangle)$	2	y	y	
-2	$(\|0\rangle\|\text{-}2\rangle+\|\text{-}2\rangle\|0\rangle)$, $\|\text{-}1\rangle\|\text{-}1\rangle$	2	y	y	
-3	$(\|\text{-}1\rangle\|\text{-}2\rangle+\|\text{-}2\rangle\|\text{-}1\rangle)$	1	y		
-4	$\|\text{-}2\rangle\|\text{-}2\rangle$	1	y		
		$\sum d = 15$	9	5	1

Three-quadrulpole phonon excitations

Applying the same methods, one can easily (hah!) show, that the conbinations give $I^\pi = 6^+, 4^+, 3^+, 2^+, 0^+$.

She Krane's Figure 5.19, p. 141, for evidence of phonon excitation.

Nuclear Rotations (Rotons)

Nuclei in the mass range $150 < A < 190$ and $A > 200$ have permanent non-spherical deformations. The quadrupole moments of these nuclei are larger by about an order of magnitude over their non-deformed counterparts.

This permanent deformation is usually modeled as follows:

$$R_N(\theta) = R_{\text{avg}}[1 + \beta Y_{20}(\theta)] \ . \tag{12.17}$$

β is called the deformation parameter. β is called the deformation parameter, (12.17) describes (approximately) an ellipse. (This is truly only valid if β is small. β is related to the eccentricity of an ellispe as follows,

$$\beta = \frac{4}{3}\sqrt{\frac{\pi}{5}}\frac{\Delta R}{R_{\text{avg}}} \ , \tag{12.18}$$

where ΔR is the difference between the semimajor and semiminor axes of the ellipse. When $\beta > 0$, the nucleus is a *prolate* ellipsoid (cigar shaped). When $\beta < 0$, the nucleus is an *oblate* ellipsoid (shaped like a curling stone). Or, if you like, if you start with a spherical blob of putty and roll it between your hands, it becomes prolate. If instead, you press it between your hands, it becomes oblate.

The relationship between β and the quadrupole moment[2] of the nucleus is:

$$Q = \frac{3}{\sqrt{5\pi}} R_{\text{avg}}^2 Z\beta \left[1 + \frac{2}{7}\left(\frac{5}{\pi}\right)^{1/2}\beta + \frac{9}{28\pi}\beta^2\right] \ . \tag{12.19}$$

Energy of rotation

Classically, the energy of rotation, E_{rot} is given by:

$$E_{\text{rot}} = \frac{1}{2}\mathcal{I}\omega^2 \ , \tag{12.20}$$

where $\mathcal{I}$ is the *moment of interia* and ω is the rotational frequency. The transition to Quantum Machanics is done as follows:

$$E_{\text{rot}}^{\text{QM}} = \frac{1}{2}\frac{\vec{\mathcal{I}}\cdot\vec{\mathcal{I}}}{\mathcal{I}}\omega^2 = \frac{1}{2}\frac{(\vec{\mathcal{I}}\omega)\cdot(\vec{\mathcal{I}}\omega)}{\mathcal{I}} = \frac{1}{2}\frac{\langle(\vec{I}\hbar)\cdot(\vec{I}\hbar)\rangle}{\mathcal{I}} = \frac{\hbar^2}{2\mathcal{I}}\langle\vec{I}\cdot\vec{I}\rangle = \frac{\hbar^2}{2\mathcal{I}}I(I+1) \tag{12.21}$$

Technical aside:

Moment of Interia?

Imagine that an object is spinning around the z-axis, which cuts through its center of mass, as shown in Figure 12.15. We place the origina of our coordinate system at the object's center of mass. The angular frequency of rotation is ω.

The element of mass, $\mathrm{d}m$ at $\vec{x}$ is $\rho(\vec{x})\mathrm{d}\vec{x}$, where $\rho(\vec{x})$ is the mass density. $[M = \int \mathrm{d}\vec{x}\,\rho(\vec{x})]$. The speed of that mass element, $|v(\vec{x})|$ is $\omega r\sin\theta$. Hence, the energy of rotation, of that element of mass is:

$$\mathrm{d}E_{\text{rot}} = \frac{1}{2}\mathrm{d}m\,|v(\vec{x})|^2 = \frac{1}{2}\mathrm{d}\vec{x}\,[\rho(\vec{x})r^2\sin^2\theta]\omega^2 \ . \tag{12.22}$$

Integrating over the entire body gives:

[2]Krane's (5.16) is incorrect. The β-term has a coefficient of 0.16, rather than 0.36 as impliced by (12.19). Typically, this correction is about 10%. The additional term provided in (12.19) provides about another 1% correction.

Figure 12.15: A rigid body in rotation. (Figure needs to be created.)

$$E_{\rm rot} = \frac{1}{2}\mathcal{I}\omega^2 \ , \tag{12.23}$$

which defines the moment of interia *to be:*

$$\mathcal{I} = \int {\rm d}\vec{x}\, \rho(\vec{x}) r^2 \sin^2\theta \ . \tag{12.24}$$

The moment of inertia is an intrinisic property of the object in question.

Example 1: Moment of inertia for a spherical nucleus

Here,

$$\rho(\vec{x}) = M\frac{3}{4\pi R_N^3}\Theta(R_N - r) \ .$$

Hence,

$$\begin{aligned}
\mathcal{I}_{\rm sph} &= M\frac{3}{4\pi R_N^3}\int_{|\vec{x}|\le R_N} {\rm d}\vec{x}\, r^2\sin^2\theta \\
&= \frac{3M}{2R_N^3}\int_0^{R_N} {\rm d}r\, r^4 \int_0^{\pi} \sin\theta {\rm d}\theta\, \sin^2\theta \\
&= \frac{3MR_N^2}{10}\int_{-1}^{1} {\rm d}\mu\,(1-\mu^2) \\
\mathcal{I}_{\rm sph} &= \frac{2}{5}MR_N^2
\end{aligned} \tag{12.25}$$

Example 2: Moment of inertia for an elliptical nucleus

Here, the mass density is a constant, but within a varying radius given by (12.17), namely

$$R_N(\theta) = R_{\rm avg}[1+\beta Y_{20}(\theta)]\ .$$

The volume of this nucleus is given by:

$$\begin{aligned}
V &= \int_{|\vec{x}|\le R_{\rm avg}[1+\beta Y_{20}(\mu)]} {\rm d}\vec{x} \\
&= 2\pi\int_{-1}^{1}{\rm d}\mu \int_0^{R_{\rm avg}[1+\beta Y_{20}(\mu)]} r^2{\rm d}r \\
&= \frac{2\pi R_{\rm avg}^3}{3}\int_{-1}^{1}{\rm d}\mu\,[1+\beta Y_{20}(\mu)]^3
\end{aligned} \tag{12.26}$$

$$\begin{aligned}
\mathcal{I}_\ell &= \int {\rm d}\vec{x}\,\rho(\vec{x}) r^2\sin^2\theta \\
&= \frac{M}{V}(2\pi)\int_{-1}^{1}{\rm d}\mu\,(1-\mu^2)\int_0^{R_{\rm avg}[1+\beta Y_{20}(\mu)]} {\rm d}r\, r^4 \\
&= \frac{MR_{\rm avg}^5}{V}\frac{2\pi}{5}\int_{-1}^{1}{\rm d}\mu\,(1-\mu^2)[1+\beta Y_{20}(\mu)]^5 \\
\mathcal{I}_\ell &= MR_{\rm avg}^2\left(\frac{3}{5}\right)\left[\int_{-1}^{1}{\rm d}\mu\,(1-\mu^2)[1+\beta Y_{20}(\mu)]^5\right] \Big/ \left[\int_{-1}^{1}{\rm d}\mu\,[1+\beta Y_{20}(\mu)]^3\right]
\end{aligned} \tag{12.27}$$

(12.27) is a ratio a $5^{\rm th}$-order polynomial in β, to a $3^{\rm rd}$-order polynomial in β. However, it can be shown that it is sufficient to keep only $O(\beta^2)$. With,

$$Y_{20}(\mu) = \sqrt{\frac{5}{16\pi}}(3\mu^2 - 1)$$

(12.27) becomes:

$$\begin{aligned} \mathcal{I}_\ell &= \left(\frac{2}{5}\right) MR_{\rm avg}^2 \left[1 - \frac{1}{2}\sqrt{\frac{5}{\pi}}\beta + \frac{71}{28\pi}\beta^2 + O(\beta^3)\right] \\ &= \left(\frac{2}{5}\right) MR_{\rm avg}^2 \left[1 - 0.63\beta + 0.81\beta^2 + (< 1\%)\right] \ . \end{aligned} \tag{12.28}$$

Rotational bands

$E_{\rm rot}(I^\pi)$	Value	Interpretation
$E(0^+)$	0	ground state
$E(2^+)$	$6(\hbar^2/2\mathcal{I})$	1st rotational state
$E(4^+)$	$20(\hbar^2/2\mathcal{I})$	2nd rotational state
$E(6^+)$	$42(\hbar^2/2\mathcal{I})$	3rd rotational state
$E(8^+)$	$72(\hbar^2/2\mathcal{I})$	4th rotational state
$\vdots$	$\vdots$	$\vdots$

Using $\mathcal{I}_{\rm rigid}$, assuming a rigid body, gives a spacing that is low by a factor of about off by about 2–3. Using

$$\mathcal{I}_{\rm fluid} = \frac{9}{8\pi} M_N R_{\rm avg}^2 \beta$$

for a fluid body in rotation[3], gives a spacing that is high by a factor of about off by about 2–3. Thus the truth for a nucleus, is somewhere in between:

$$\mathcal{I}_{\rm fluid} < \mathcal{I}_N < \mathcal{I}_{\rm rigid}$$

[3]Actually, the moment of inertia of a fluid body is an ill-defined concept. There are two ways I can think of, whereby the moment of inertia may be reduced. One model could be that of a "static non-rotating core". From (12.29), this would imply that:

$$\mathcal{I}_\ell = -\left(\frac{2}{5}\right) M R_{\rm avg}^2 \left[\frac{1}{2}\sqrt{\frac{5}{\pi}}\beta - \frac{71}{28\pi}\beta^2\right] \approx -\left(\frac{2}{5}\right) M R_{\rm avg}^2 \left[\beta - 0.81\beta^2\right] \ .$$

Another model would be that of viscous drag, whereby the angular frequency becomes a function of r and θ. For example, $\omega = \omega_0(r\sin\theta/R_{\rm avg})^n$. One can show that the reduction, R_n in $\mathcal{I}$ is of the form $R_{n+1} = \frac{2(n+2)}{7+2n} R_n$, where $R_0 \equiv 1$. A "parabolic value", $n = 2$, gives the correct amount of reduction, about a factor of 3. This also makes some sense, since rotating liquids obtain a parabolic shape.